ADVANCED MATERIALS

gels are spontaneously formed. Energy migration from the membrane-bound $NaphSO_3^-$ to $AnthSO_3^-$ *in aqueous dispersions* is restricted by the lower surface concentration of $NaphSO_3^-$. In the hydrogel state (above 3 mM), $NaphSO_3^-$ chromophores accumulate on the fibrous nanoassemblies and their bundling and crosslinking make them into light-harvesting supramolecular networks.

The formation of self-assembling hydrogels has received considerable interest recently.[17,18] However, the design of functional hydrogels is largely unexplored. This is because it is difficult to induce the formation of crosslinked fibrous aggregates rather than precipitation in water. In this study, we have shown that a series of less-hydrophobic ammonium amphiphiles acquire sufficient amphiphilicity upon complexation with hydrophobic anions to hierarchically self-assemble into photofunctional hydrogels. The importance of supramolecular amphiphilicity is a common feature of complementary hydrogen-bond directed mesoscopic supramolecular assemblies.[19] The present approach not only provides a rational design for self-assembling hydrogels but also allows organization of functional molecules that *alone* do not show self-assembling properties. We envisage that light-harvesting hydrogels might play an important role in the development of artificial eye lenses and serve as unique matrices for the photoregulation of protein functions.[20]

Experimental

Preparation of Supramolecular Hydrogels: To ensure homogeneous mixing, the equimolar mixtures (hydrogels) were either ultrasonicated for 1–2 min or heated to 80 °C. The supramolecular hydrogels were reversibly formed by placing the sols containing **1** and **2** at room temperature. The hydrogel of **1**/$NaphSO_3^-$ displayed shrinkage to almost half of the initial volume after about 3 days, while that formed by **2**/$AnthSO_3^-$ is stable at room temperature for a period of 3 months.

Gel-Transfer Experiment: Freshly cleaved HOPG was lightly pressed against the gel surfaces and allowed to stand for 15 min. The substrates were then detached from the gel surfaces and observed by AFM (Topometrix TMX-2100, non-contact mode) [2,11].

Fluorescence Measurement of Aqueous Dispersions and Hydrogels: The samples were excited with an incidence angle of 45° to the quartz cell surface and the fluorescence was detected along the normal. Naphthalene chromophores were selectively excited at an excitation wavelength of 290 nm.

Ultrafiltration Binding Assay: Ultrafiltration was conducted for aqueous dispersions or gels of **1**/$NaphSO_3^-$ (concentration 5×10^{-5} M to 5 mM) by using a MOLCUT II filter (NIHON Millipore LTD, molecular cut-off weight 10^4). The concentration of the unbound chromophores was determined by measuring the absorbance (at 273 nm) of the filtered aqueous solutions.

Received: February 15, 2002
Final version: May 6, 2002

[1] W. Kühlbrandt, D. N. Wang, *Nature* **1991**, *350*, 130.
[2] N. Kimizuka, M. Shimizu, S. Fujikawa, K. Fujimura, M. Sano, T. Kunitake, *Chem. Lett*. **1998**, 967.
[3] a) N. Nakashima, A. Tsuge, T. Kunitake, *J. Chem. Soc., Chem. Commun*. **1985**, 41. b) Y. Ishikawa, T. Kunitake, *J. Am. Chem. Soc*. **1991**, *113*, 621.
[4] T. Kunitake, A. Tsuge, N. Nakashima, *Chem. Lett*. **1984**, 1783.
[5] a) E. W. Kaler, A. K. Murthy, B. E. Rodriguez, J. A. N. Zasadzinski, *Science* **1989**, *245*, 1371. b) R. A. Salkar, D. Mukesh, S. D. Samant, C. Manohar, *Langmuir* **1998**, *14*, 3778.
[6] Ion pairs of 3-hydroxynaphthalene-2-carboxylate and cetyltrimethyl-ammonium form vesicles and worm-like micelles, but hydrogels are not formed. R. A. Salkar, P. A. Hassan, S. D. Samant, B. S. Valaulikar, V. V. Kumar, F. Kern, S. J. Candau, C. Manohar, *Chem. Commun*. **1996**, 1223.
[7] T. Kunitake, *Angew. Chem. Int. Ed. Engl.* **1992**, *31,* 709.
[8] N. Kimizuka, M. Tokuhiro, H. Miyauchi, T. Wakiyama, T. Kunitake, *Chem. Lett*. **1997**, 1049.
[9] Once the hydrogel is formed, the test tube filled with the mixture can be turned upside down without any flow.
[10] The minimum concentration for gelation is about 5 mM for **1**/1-naphthalene sulfonate, **1**/styrene sulfonate, and **1**/perchlorate. **1**/$AnthSO_3^-$ precipitates at a concentration of 5 mM.
[11] a) N. Kimizuka, S. Fujikawa, T. Kunitake, *Adv. Mater*. **1998**, *10*, 1373. b) N. Kimizuka, S. Fujikawa, T. Kunitake, *Chem. Lett*. **1998**, 821.
[12] a) I. B. Berlman, *Energy Transfer Parameters of Aromatic Compounds*, Academic Press, New York **1973**. b) J. B. Birks, *Photophysics of Aromatic Molecules*, Wiley-Interscience, London **1969**. c) M. Kasha, in *Spectroscopy of the Excited State* (Ed: B. D. Bartolo), Plenum Press, New York **1976**, p. 337. d) V. L. Levschin, E. G. Baranova, *Opt. Spectrosc*. **1959**, *6*, 31. e) N. Nakashima, N. Kimizuka, T. Kunitake, *Chem. Lett*. **1985**, 1817.
[13] N. Kimizuka, T. Kunitake, *J. Am. Chem. Soc*. **1989**, *111*, 3758.
[14] T. Förster, *Ann. Phys.* (*Leipzig*) **1948**, *2*, 55.
[15] a) N. Nakashima, R. Ando, T. Kunitake, *Bull. Chem. Soc. Jpn*. **1987**, *60*, 1967. b) B. Armitage, P. A. Klekotka, E. Oblinger, D. F. O'Brien, *J. Am. Chem. Soc*. **1993**, *115*, 7920.
[16] D. A. Holden, J. E. Guillet, *Macromolecules* **1982**, *15*, 1475. The Förster radius for naphthalene–anthracene energy transfer is about 24 Å [12a].
[17] a) R. Oda, I. Huc, S. J. Candau, *Angew. Chem. Int. Ed.* **1998**, *37*, 2689. b) L. A. Estroff, A. D. Hamilton, *Angew. Chem. Int. Ed.* **2000**, *39*, 3447. c) F. M. Menger, K. L. Caran, *J. Am. Chem. Soc*. **2000**, *122*, 11 679. d) S. Bhattacharya, S. N. G. Acharya, *Chem. Mater*. **1999**, *11*, 3504. e) S. Franceschi, N. de Viguerie, M. Riviere, A. Lattes, *New J. Chem*. **1999**, *23*, 447. f) M. Amaike, H. Kobayashi, S. Shinkai, *Chem. Lett*. **2001**, 620.
[18] Physical gelation of organic solvents by small molecules has been extensively studied. For example: P. Terech, R. G. Weiss, *Chem. Rev.* **1997**, *97*, 3133.
[19] T. Kawasaki, M. Tokuhiro, N. Kimizuka, T. Kunitake, *J. Am. Chem. Soc*. **2001**, *123*, 6792.
[20] N. Kimizuka, A. Baba, T. Kunitake, *J. Am. Chem. Soc*. **2001**, *123*, 1764.

Control of the Magnetic Anisotropy of a Co/Pt Nanomultilayer with Embedded Particles**

By *In-Joon Jeon*, *Dong-Wook Kang*, *Dong-Eon Kim*,* *Dong-Hyun Kim*, *Sug-Bong Choe*, and *Sung-Chul Shin*

Ever-demanding miniaturization has now reached a point where the dimensions of components in a device are in the nanometer scale.[1,2] However, the working principle on such a scale may not be the same as on larger scales and is governed by quantum phenomena. The successful application of nanotechnology depends upon the detailed understanding of phenomena in the nanometer regime and the acquirement of control of the fabrication and manipulation of nanostructural building blocks such as nanomultilayers (nano-MLs), nanowires and nanoparticles. Efforts in recent years, have focused on the fabrication and characterization of nanostructures and

[*] Prof. D.-E. Kim, Dr. I.-J. Jeon, D.-W. Kang
Physics Department and Electron Spin Science Center
Pohang University of Science and Technology
Pohang, Kyungbuk 790-784 (Korea)
E-mail: kimd@postech.ac.kr
D.-H. Kim, Dr. S.-B. Choe, Prof. S.-C. Shin
Department of Physics and Center for Nanospinics of Spintronic Materials
Korea Advanced Institute of Science and Technology
Taejon 305-701 (Korea)

[**] This work was supported in part by the Electron Spin Science Center, funded by The Korean Scientific and Engineering Foundation and by the POSTECH BSRI research fund and by the Brain Korea 21 project.

  0935-9648/02/1608-1116 $ 17.50+.50/0

their subsequent manipulation.[3–18] Magnetic nanoparticles can affect the electron conduction or optical properties of their host, and in turn the host may have an effect on the magnetic properties of the nanoparticles.[14–18] The fabrication of microelectronics with the capability of recording and data storage, along with spin-dependent switching, may be possible by utilizing and embedding magnetic particles into semiconductors. Since a Co/Pt nano-ML system has been studied as a magneto-optical (MO) material and is known to show the uni-axial magnetic anisiotropy, it has been chosen for the manipulation of its magnetic anisotropy. The particle and nano-ML effects have been combined to tailor the magnetic properties of Co/Pt ML films. We demonstrate for the first time that the control of layer thickness and the embedment of particles can change the nature of a magnetic anisotropy: from the uni-axial to the bi-axial state. The samples, fabricated by a newly developed normal incidence pulsed laser deposition (NIPLD) method,[19] have salient magnetic characteristics, differing from particle-free samples of almost the same structure: a) they exhibit bi-axial magnetic anisotropies and b) there exists a critical field at which the easy direction of magnetization changes from a parallel direction (to the sample surface) to a perpendicular direction and vice versa. By a careful manipulation of particles and nanolayers, we also demonstrate control of the degree of magnetic anisotropy by embedding particles in a well-defined nanomultilayer system: control between a uni-axial anisotropy and a bi-axial one and vice versa. This work is a clear demonstration of the tailoring of the properties of nanostructures with particles.

Co/Pt nano-MLs were prepared on a native oxide Si (100) wafer under a base pressure of ~1×10^{-6} torr at room temperature (RT) by NIPLD.[19] The sample was fabricated with a laser fluence of 0.38 J/cm^2 for Co and 0.42 J/cm^2 for Pt. In conventional pulsed laser deposition (PLD), ablating laser beams are directed onto a target at an incidence angle of 45°. During deposition, the direction of the laser plume changes because the craters made by laser ablation modify the surface. Hence, using conventional PLD, it has been very difficult to produce uniform, well-defined MLs with a thickness of a nanometer or less. The use of NIPLD has overcome this problem, and enables one to fabricate excellent ML layers with layer thicknesses of a few tenths of a nanometer. The nano-MLs fabricated by NIPLD in this study have 15 bi-layers. The thickness of the Co layer varies from 0.4–0.8 nm and that of the Pt layer is ~1 nm. We have chosen these thicknesses because it has been known that a ML system with a Co-layer thickness of ~0.5 nm and a Pt-layer thickness of ~1 nm has a uni-axial perpendicular (to its ML surface) magnetic anisotropy.

Small-angle X-ray scattering (SAXS) using Cu Kα radiation at 0.154 nm was used to characterize the structures of the samples. The SAXS data of one sample, shown in Figure 1, reveals sharp Bragg peaks and clear Kiessig fringes, indicating that the layer thickness is uniform and the interface roughness is small. The fitting (the solid line) was performed using the dynamical X-ray scattering theory,[20,21] which showed that the thicknesses of the Co and Pt layers are 0.6 and 1.3 nm, respectively. The inset in Figure 1a is the large-angle X-ray scattering data, showing that the growth direction of Pt is <111> and that the Co layers do not have any crystalline structure. The structural parameters, determined by SAXS, are: d_{Co} = 0.4 nm, $d_{Pt} = 1.1$ nm for S1 and S2; $d_{Co} = 0.6$ nm, $d_{Pt} = 1.3$ nm for S3; $d_{Co} = 0.7$ nm, $d_{Pt} = 1.0$ nm for S4.

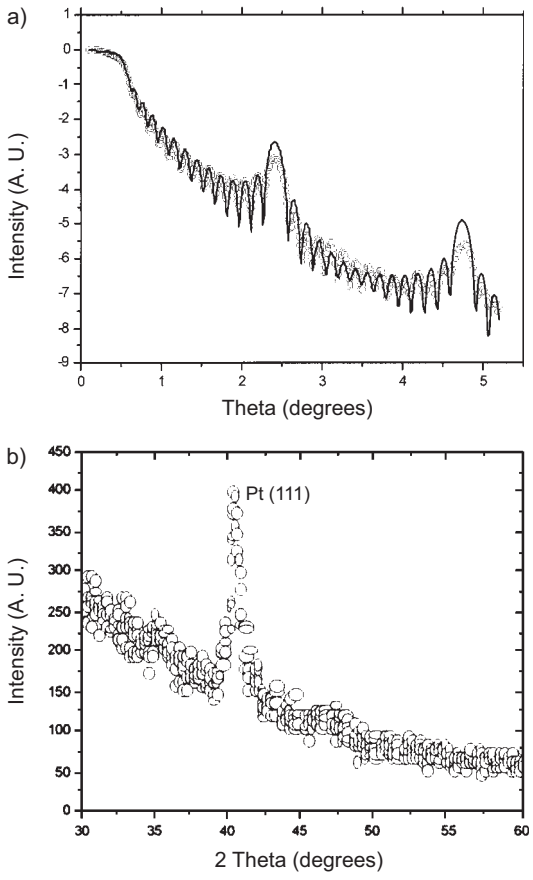

Fig. 1. a) Structural analysis: small-angle X-ray scattering data (○) of sample S2, showing the well-defined nanomultilayer structure. The thicknesses of the Co and Pt layers are estimated to be 0.57 and 1.3 nm, respectively, by fittings (solid line) using X-ray dynamical scattering theory. b) Large-angle X-ray scattering data, indicating that Pt has a crystalline structure and Co does not.

The production of particles using PLD has been known for some time. The careful control and minimizing of the laser energy impinging onto a target can lead to the reduction of the number of particles as well as the decrease of their average size. The laser energies used were 90 and 105 mJ for Co and Pt, respectively, for which the deposition rates were about 2.3×10^{-4} nm/shot for Co and 4.3×10^{-4} nm/shot for Pt. The scanning electron microscopy (SEM) measurement reveal that at this level of the deposition process, a majority of the particles are in the size range of a few to a few tens of nanometers in diameter, with an estimated density of 1.1×10^9 particles/cm^2. The density of larger particles is smaller, typically less than 10^6 particles/cm^2. During the deposition process, these particles, which are first formed and deposited as atoms, subsequently form layers. Hence a nano-ML with embedded particles is fabricated. These particles cover about 10 % of a sample area.

  0935-9648/02/1608-1117 $ 17.50+.50/0

ADVANCED MATERIALS

The magnetic properties of our samples were characterized by use of a vibrating sample magnetometer (VSM) and a null-type torque magnetometer (TM). Figure 2 shows the magnetization behavior (Figs. 2a–d) measured by VSM and the torque measurements (Figs. 2e–h) at RT with an applied field of 10 kOe. Each row represents one sample: depicting its magnetization and corresponding torque measurements. The first sample (S1, Figs. 2a,e) is different from other samples in that it has 10 bi-layers and was fabricated using a magnetron sputtering system where atoms are sputtered and deposited onto a substrate. This sample is then free of particles. The SAXS measurement of S1 revealed that it has almost the same structure as S2. The magnetization measurements were performed with an applied magnetic field perpendicular (red dots and lines) and parallel (blue open circles and lines) to the ML surface. As shown in Figure 2a, S1 reveals hysteresis only in the perpendicular direction, indicating that the easy direction of magnetization is perpendicular to the ML surface. The torque measurement data closely resembles a sine function (Fig. 2e). This is a typical characteristic of the uni-axial perpendicular magnetic anisotropy of Co/Pt MLs with thicknesses of the Co- and Pt-layers being less than 1 nm, fabricated by either a magnetron sputtering or an electron-beam deposition. S2 has both similar and different features to S1. A similar feature is that its easy direction of magnetization is perpendicular to its surface; on the other hand, different features include its coercivity being smaller and its magnetic anisotropy not being uniaxial. The torque measurement cannot be fitted by a simple sine function. This effect is attributed to the nonlinear contribution from the in-plane magnetization due to particles embedded in the nano-ML, because a) from the point of view of morphology, the major difference between the samples S1 and S2 is the existence of particles, b) the amount of particles in the sample S2 is not negligible (it is in fact ca. 10 % in terms of the area ratio), and c) the VSM shows higher saturation magnetization in the parallel direction than in the perpendicular direction.

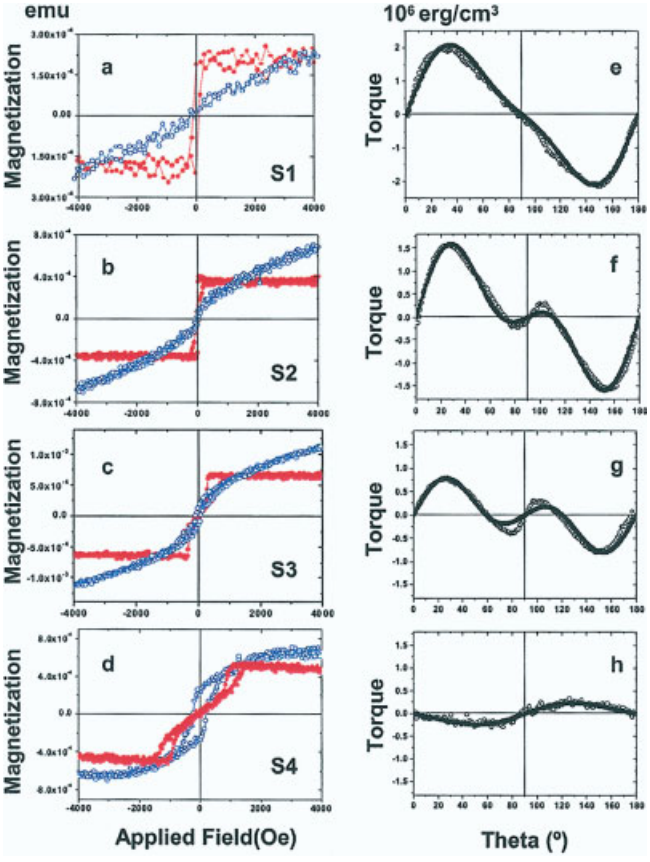

Fig. 2. Magnetization and torque measurement: the magnetizations were measured with a magnetic field parallel (blue, open circles) and perpendicular (red, closed dots) to the sample surface. The magnetic field of 10 kOe was applied in the torque measurement. S1 was fabricated using a magnetron sputtering system. All other samples were made by NIPLD. The structural parameters, determined by SAXS, are: $d_{Co} = 0.4$ nm, $d_{Pt} = 1.1$ nm for S1 and S2; $d_{Co} = 0.6$ nm, $d_{Pt} = 1.3$ nm for S3; $d_{Co} = 0.7$ nm, $d_{Pt} = 1.0$ nm for S4.

The torque measurements of these samples also indicate the change of their magnetic anisotropy properties. If the perpendicular magnetic anisotropy (PMA) due to interfacial effects in the ML structure and the in-plane anisotropy due to particles embedded in the ML were independent, the magnetic anisotropy energy E_a could be written as:

$$E_a(\theta) = K_{eff\_ML} \sin^2(\theta) + K_{eff\_par} \sin^2(90-\theta) - M_S H \quad (1)$$

where K_{eff_ML} and K_{eff_par} are the effective anisotropy constants due to the ML system and particles, respectively. K_{eff_ML} includes the contributions from both bulk and interfaces. θ is the angle between the surface and an applied magnetic field (H). M_S is the saturation magnetization. The torque would then be expressed by

$$\Gamma = -\frac{dE_a(\theta)}{d\theta} = (K_{eff\_ML} - K_{eff\_par}) \sin(2\theta). \quad (2)$$

The shape of the torque curve is basically that of $\sin(2\theta)$ and the relative strength of the anisotropy constants determines the magnitude and direction of the torque. However, the measured torque curve is substantially different from this. Hence the shape of the curve indicates the additional nonlinear effect. Including this effect as the next higher-order term, then the magnetic anisotropy energies $E_a(\theta)$ are written as follows:

$$E_a(\theta) = K_{eff\_ML} \sin^2(\theta) + K_{eff\_par} \sin^2(90-\theta) - M_S H + K_2 \sin^4(\theta) \quad (3)$$

$$\Gamma = -\frac{dE_a}{d\theta} = -K_{eff} \sin(2\theta) - 2K_2 \sin^2(\theta) \sin(2\theta). \quad (4)$$

where $K_{eff} = K_{eff\_ML} - K_{eff\_par}$ and K_2 is the second-order anisotropy constant. It is assumed here that the direction of magnetization is almost the same as that of an applied magnetic field.

Samples with different thicknesses of Co layers were also fabricated under the same conditions as for S2. As the thickness of a Co layer increases (or the number of Co particles

  0935-9648/02/1608-1118 $ 17.50+.50/0

increases), the ferromagnetic characteristics (hysteresis in magnetization) are developed in the direction parallel to its surface; on the other hand, in the perpendicular direction, the ferromagnetic behavior diminishes (no coercivity field). A salient feature is that there exists a critical magnetic field at which the easy direction of magnetization changes from the parallel direction to the perpendicular direction or vice versa. To our knowledge, this kind of magnetization behavior has not been observed before this.

Using Equation 4 for the magnetic anisotropy energy, the fittings (solid squares) to the experimental data (open circles) were performed (Figs. 2e–h) to determine the anisotropy constants, and the results are displayed in Figure 3. The fitting shows that the sign of K_2 is negative, the meaning of which is

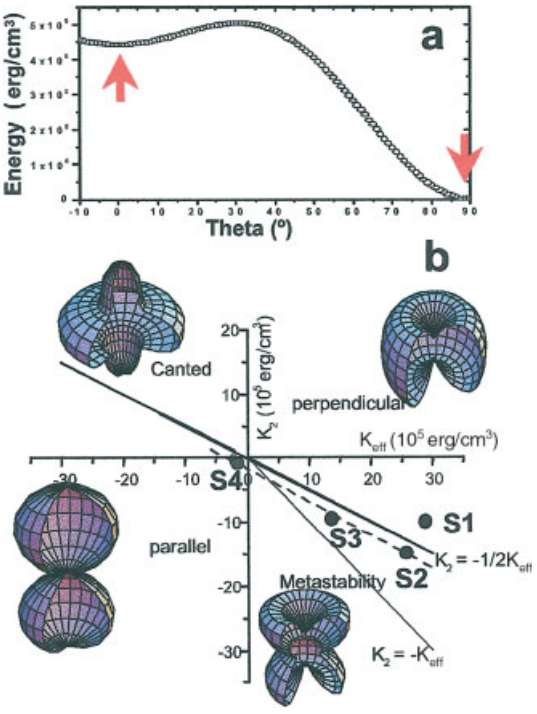

Fig. 3. Magnetic anisotropy and phase diagram: a) magnetic anisotropy energy of S3, b) magnetic phase diagram. S2 and S3 fabricated by NIPLD fall in the meta-stable region where the parallel direction becomes an additional easy direction.

clear in the plot of $E_a(\theta)$ as shown in Figure 3a for S3. $E_a(\theta)$ has two minima at $\theta = 0°$ (parallel) and $\theta = 90°$ (perpendicular), which is a good evidence for the existence of two easy directions for magnetization, i.e., bi-axial magnetic anisotropy.

Figure 3b is a magnetic phase diagram depicting the space of K_{eff} and K_2. Depending on the values of K_{eff} and K_2, the space is divided into 4 phases.[22–24] The line for $K_2 = -K_{eff}/2$ divides the right-hand region into the perpendicular and the meta-stable magnetization phase, and also the left-hand region into the canted and the parallel magnetization phase. A representative magnetic anisotropy energy surface of each zone is also shown. The solid dots are the data for the samples studied in this work. The sample prepared by a magnetron sputtering system falls in the region above the line $K_2 = -K_{eff}/2$. Two samples made by NIPLD fall in the meta-stable region where both the parallel and the perpendicular magnetization coexist. The effect of the existence of particles is manifested in such a way that the data points fall in the meta-stable region. The increase in the thickness of the Co layer decreases the magnitude of K_2 and makes K_{eff} negative, which means that the easy direction for the magnetization becomes parallel to the sample surface as in the case of S4.

In conclusion, Co/Pt nano-MLs with embedded particles were fabricated and have been shown to have different magnetic characteristics from particle-free samples (made by a magnetron sputtering system) of almost the same structure, especially with respect to the following matters: (1) they have smaller coercivity fields, (2) they have bi-axial magnetic anisotropies and (3) there exists a critical field at which the easy direction changes from the parallel direction to a perpendicular direction and vice versa. This work demonstrates the capability of engineering a magnetic anisotropy from a uni-axial type to a bi-axial one and vice versa, via the combination of particles and nanolayers. The further development of this capability leads to a new type of nanomagnetic switch. This work clearly shows that the integration of nanobuilding blocks into nanostructures can result in the tailoring of the properties of nanomaterials.

Experimental

Uniform, well-defined MLs in which each layer has a thickness of a nanometer or less are very difficult to fabricate using a pulsed laser deposition at an incidence angle of 45° because the direction of the laser plume changes during the deposition, due to the modification of the laser target surface, resulting in the variation of the deposition rate. Thus NIPLD has been developed and enables one to fabricate excellent ML layers with layers of a few tenths of nanometers [19]. In this experiment, Co/Pt nano-MLs was fabricated by NIPLD on a native oxide Si (100) wafer under a base pressure of ~ 1×10^{-6} torr at RT. A pulsed (5 ns full-width at half-maximum), second-harmonic Nd/YAG laser (532 nm light) operating at 10 Hz was focused on Co and Pt targets with a laser fluence of 0.38 J/cm^2 and 0.42 J/cm^2, respectively. The separation between a substrate and the laser target was 7 cm, and the distance between the laser axis and the sample substrate was 2.7 cm. The deposition rates were about 2.3×10^{-4} nm/shot for Co and 4.3×10^{-4} nm/shot for Pt. This calibration was performed by thickness measurements of single and multilayer test samples with SAXS. The number of laser shots or the laser operation time controlled the thickness. Before deposition, the laser was rastered over a target to clean the target surface for 1 or 2 h. During this cleaning process, the shutter was closed to keep a sample from any contamination.

The multilayer structures were analyzed by SAXS measurements (the conventional θ–2θ scan) using Cu Kα radiation at 0.154 nm from a rotating anode X-ray tube (Rigaku, RU300; the output power used is 8 kW) with an angular resolution of 0.01–0.02° (the maximum angular resolution of the goniometer system is 5×10^{-5}°). The data fitting for the estimation of structural parameters was made by using a computer code based on X-ray dynamical scattering theory which takes into account multiple scatterings by interfaces in a multilayer system.[20,21]

The magnetization measurement was performed using a vibrating sample magnetometer (Lakeshore, 7300 series). The magnetic field was swept between ± 4 kOe (maximum: 8 kOe) with a sweep duration of 10 min.

The magnetic anisotropy was measured by a null-type homemade torque magnetometer, having a resolution of 5×10^{-4} dyn cm in the measurement range of ±15 dyn cm. This system has been tested and is seen to perform excellently [25]. The measurements were carried out at RT with a magnetic field of 10 kOe. The small signal from the sample holder and uncoated substrate was subtracted for the torque analysis.

Received: March 4, 2002
Final version: May 7, 2002

  0935-9648/02/1608-1119 $ 17.50+.50/0

ADVANCED MATERIALS

[1] P. Peercy, *Nature* **2000**, *406*, 1023.
[2] G. Timp, *Nanotechnology*, Springer-Verlag, New York **1999**.
[3] C. Dekker, *Phys. Today* **1999**, *52*, 22.
[4] S. J. Tans, T. M. Verschueren, C. Dekker, *Nature* **1998**, *393*, 49.
[5] J. Hu, M. Ouyang, P. Yang, C. M. Lieber, *Nature* **1999**, *399*, 48.
[6] X. Duan, Y. Huang, Y, Cui, J. Wang, C. M. Lieber, *Nature* **2001**, *409*, 66.
[7] Y. Cui, C. M. Lieber, *Science* **2001**, *291*, 851.
[8] T. Thurn-Albrecht, J. Schotter, G. A. Kästle, N. Emley, T. Shibauchi, L. Krusin-Elbaum, K. Guarini, C. T. Black, M. T. Tuominen, T. P. Russell, *Science* **2000**, *290*, 2126.
[9] Y. R. Hacohen, E. Grunbaum, R. Tenne, J. Sloan, J. L. Hutchison, *Nature* **1998**, *395*, 336.
[10] A. P. Alivisatos, *Science* **1996**, *271*, 933.
[11] S. Indris, P. Heitjans, H. E. Roman, A. Bunde, *Phys. Rev. Lett.* **2000**, *84*, 2889.
[12] T. Bachels, T. Schafer, H. J. Guntherodt, *Phys. Rev. Lett.* **2000**, *84*, 4890.
[13] A. A. Shvarstburg, M. F. Jarrold, *Phys. Rev. Lett*. **2000**, *85*, 2530.
[14] H. Sato, O. Kitakami, T. Sakurai, Y, Shimada, *J. Appl. Phys.* **1997**, *81*, 1858.
[15] R. H. Kodama, A. S. Edelstein, *J. Appl. Phys.* **1999**, *85*, 4316.
[16] K. J. Kirk, J. N. Chapman, S. McVitie, P. R. Aitchison, C. D. W. Wilkinson, *Appl. Phys. Lett*. **1999**, *75*, 3683.
[17] G. M. Pastor, J. Dorantes-Davila, S. Pick, H. Dreysse, *Phys. Rev. Lett*. **1995**, *75*, 326.
[18] B. J. Hickey, M. A. Howson, S. O. Musa, N. Wiser, *Phys. Rev. B* **1995**, *51*, 667.
[19] I. J. Jeon, D. Kim, D. J. S. Song, J. H. Her, D. R. Lee, K.-B. Lee, *Appl. Phys. A* **2000**, *70*, 235.
[20] D. R. Lee, Y. J. Park, D. Kim, Y. H. Jeong, K.-B. Lee, *Phys. Rev. B* **1998**, *57*, 8786.
[21] D. Kim, D. Cha, S. Lee, *J. Vac. Sci. Technol. A* **1997**, *154*, 2291.
[22] A. Hucht, K. D. Usadel, *Phys. Rev. B* **1997**, *55*, 12 309.
[23] Y. Millev, J. Kirschner, *Phys. Rev. B* **1996**, *54*, 4137.
[24] H. Fritzsche, J. Kohlepp, H. J. Elmers, U. Gradmann, *Phys. Rev. B* **1994**, *49*, 15 665.
[25] a) S.-C. Shin, J.-H. Kim, D.-H. Ahn, *J. Appl. Phys.* **1991**, *69*, 5664. b) J. Hur, S.-C. Shin, *Appl. Phys. Lett.* **1993**, *62*, 2140.

Nanocomposite Hydrogels: A Unique Organic–Inorganic Network Structure with Extraordinary Mechanical, Optical, and Swelling/De-swelling Properties**

By *Kazutoshi Haraguchi** and *Toru Takehisa*

In the last two decades, polymeric hydrogels, such as poly(*N*-isopropyl acrylamide) (PNIPA) gel, that display a sensitivity to external stimuli (e.g., temperature, solvent composition, pH, light, pressure, magnetic, and electric fields) have attracted much scientific interest and have been used in many applications.[1–3] However, they have several significant limitations due to their chemically crosslinked network structures. Since the dawn of the science of polymer networks,[4,5] a major goal has been to control the crosslinking density ν (= number of crosslinked chains per unit volume) and the inter-crosslinking molecular weight M_c (i.e., the chain lengths between crosslinking points) independently. However, in conventional syntheses, independent control of these parameters was a contradiction because an increase in ν was always accompanied by a decrease in M_c ($\nu \propto M_c^{-1}$). Also, since the crosslinking reaction (using crosslinking agents) could not occur at regularly separated positions, the chain lengths between crosslinking points always had a broad distribution, as shown in Figure 1C. Furthermore, structural inhomogeneity (i.e., the heterogeneous aggregation of crosslinking points) always occurred when the concentration of crosslinker was high.[6] Therefore, hydrogels composed of chemically crosslinked polymer networks have severe limitations such as morphological homogeneity (optical transparency) and mechanical properties.[6,7] That is, conventional organic, crosslinked, polymeric hydrogels (OR gels) always exhibit mechanically weak and brittle properties irrespective of ν and are often cloudy. Furthermore, since the polymer chains are molecularly restricted by a large number of crosslinks, they do not behave like flexible linear polymer chains in terms of their own characteristics such as sensitivity to external stimuli.[8] Thus, many potential applications of conventional OR gels have been restricted or abandoned because of these limitations.

Here, we propose a new type of polymeric hydrogel that solves these problems. The proposed hydrogel is a nanocomposite hydrogel (NC gel) composed of specific polymers and a water-swellable inorganic clay. The schematic illustration of the structural model for the NC gel is shown in Figure 1A. In the NC gel, inorganic clays are exfoliated and uniformly dispersed in an aqueous media. Then, neighboring clay sheets are connected by polymer chains χ, in other words, clay sheets act as multifunctional crosslinking agents for the polymer. Here, the inter-crosslinking distance (D_{ic}) is equivalent to the neighboring clay–clay interparticle distance. Then, D_{ic} can be determined by the clay concentration provided the clay is exfoliated and clay sheets are fixed in uniformly dispersed positions. Taking the polymer chain conformations into account, D_{ic} can be converted to M_c. On the other hand, ν, which is equivalent to the number of polymer chains χ per unit volume, is mainly determined by the polymer and the initiator concentrations at a fixed clay content.

The NC gel composed of the organic (polymer)/inorganic (clay) networks shown schematically in Figure 1A must be prepared by initiating polymerization from the clay surface. Here, it is important to mention that no organic crosslinker is used in the formation of the network structure of NC gel. It was found that the use of an organic crosslinker, *N*,*N*-methylenebisacrylamide (BIS), together with inorganic clay did not result in NC gels but in hydrogels similar to OR gels.[9–11] It is also important that the polymer chains attached to clay sheets are flexible chains, taking nearly random conformations in the ample space between clay sheets, since there are no restrictions arising from large numbers of organic crosslinks along their lengths. When a clay sheet is regarded as a kind of large crosslinker, the number of crosslinking units per unit volume in the NC gel is very different from that in a conventional OR gel. For example, a number of crosslinking units of 10 is calculated for the NC3 gel and 7500 for OR3 gel, per cubic 100 nm. In this study, hydrogels were designated as NC-*X* or OR-*Y*

[*] Dr. K. Haraguchi, T. Takehisa
Kawamura Institute of Chemical Research
631 Sakado, Sakura-shi, Chiba 285-0078 (Japan)
E-mail: hara@kicr.or.jp

[**] We thank S. Fan, J. Sano, and A. Ohbayashi for technical assistance, and R.-H. Jin for valuable discussions.

  0935-9648/02/1608-1120 $ 17.50+.50/0